

Article

A Novel Vibration Suppression Method for Welding Robots Based on Welding Pool Instability Evaluation and Trajectory Optimization

Mingtian Ma¹, Hong Lu¹ , Yongquan Zhang^{1,2,*} , Zidong Wu¹, He Huang¹, Xujie Yuan¹, Xu Feng¹, Zhi Liu³ and Zhangjie Li¹

¹ Hubei Digital Manufacturing Key Laboratory, Wuhan University of Technology, Wuhan 430070, China; wxmmt100@whut.edu.cn (M.M.); landzh@whut.edu.cn (H.L.); wuzidong@whut.edu.cn (Z.W.); huanghe@whut.edu.cn (H.H.); 283890@whut.edu.cn (X.Y.); 332765@whut.edu.cn (X.F.); anhmcy@whut.edu.cn (Z.L.)

² Hubei Tuansteel Science and Technology Research Co., Ltd., Huanggang 438000, China

³ School of Mechanical and Intelligent Manufacturing, Huanggang Normal University, Huanggang 438000, China; lz3839@126.com

* Correspondence: zhangyongquan@whut.edu.cn

Abstract: Industrial robots are widely used in welding operations because of their high production efficiency. The structure of the robot and the complex stress conditions during welding operations lead to the vibration of the end of robot, which leads to welding defects. However, current vibration suppression techniques for welding robots usually only consider the robotic performance while overlooking their impact on the welding metal forming process. Therefore, based on the influence of robot vibration on welding pool stability during the welding process, a new welding robot vibration suppression method is proposed in this paper, along with the establishment of a welding pool stability assessment model. The proposed vibration suppression algorithm is based on the optimization of the welding trajectory. To enhance the performance of the method, the Particle Swarm Optimization (PSO) algorithm is applied to optimize the joint angular velocity and angular acceleration. Finally, robot welding experiments are designed and conducted. By comparing vibration measurement data and welding quality before and after the vibration suppression, the effectiveness and stability of the proposed method are validated.

Keywords: welding robot; vibration suppression; robot dynamics trajectory optimization; welding pool fluctuation



Academic Editors: Salman Pervaiz, Ibrahim Deiab and Manoj Gupta

Received: 17 November 2024

Revised: 12 December 2024

Accepted: 26 December 2024

Published: 28 December 2024

Citation: Ma, M.; Lu, H.; Zhang, Y.; Wu, Z.; Huang, H.; Yuan, X.; Feng, X.; Liu, Z.; Li, Z. A Novel Vibration Suppression Method for Welding Robots Based on Welding Pool Instability Evaluation and Trajectory Optimization. *Technologies* **2025**, *13*, 12. <https://doi.org/10.3390/technologies13010012>

Copyright: © 2024 by the authors. Licensee MDPI, Basel, Switzerland. This article is an open access article distributed under the terms and conditions of the Creative Commons Attribution (CC BY) license (<https://creativecommons.org/licenses/by/4.0/>).

1. Introduction

The process of welding involves the manufacturing technique and technology of joining alloys or other thermoplastic materials through heating, high temperatures, or high pressure [1]. Robotics are extensively employed in welding operations, where the formation of weld seams is influenced by conditions such as the welding position. The precision and stability of robotic operations directly affect the continuity of the position and heat input during welding, thereby impacting the final quality of metal formation [2]. However, during the arc welding operations, the arc force and joint flexibility cause vibrations at the robot's end-effector. The magnitude of these vibrations is determined by the load size, the degree of flexibility, and the trajectory. These vibrations reduce the robot's operational precision. The vibration of the robot drives the vibration of the end welding gun, leading to a decrease in the stability of the metal forming process during welding and subsequently resulting in a

reduction in welding quality stability and consistency. Fluctuations in current and voltage also affect the stability of the welding process, but the impact of robot vibrations remains significant. Therefore, research into methods for suppressing end-of-robot vibrations aimed at improving the stability of the welding forming process is necessary [3–6].

Currently, active vibration suppression techniques for robots are primarily control-based, offering benefits such as a low cost, stable effectiveness, and broad applicability [7]. These techniques mainly encompass control structures and trajectory planning, with trajectory control methods demonstrating higher applicability and superior overall suppression capabilities [8,9]. Within trajectory control, algorithms such as trajectory optimization and path optimization have been developed. Tian et al. enhanced traditional optimization algorithms by targeting vibration levels to improve the vibration suppression performance of collaborative robots [10]. In addition to trajectory and path optimization, controllers designed with vibration levels as an input have been developed for better suppression performance. Kraus designed a linear quadratic regulator control with a state observer as an active vibration absorber control algorithm, achieving end-effector vibration suppression along the robot trajectory through the gain scheduling of outputs from local controllers [11]. Rsetam et al. proposed a hierarchical sliding mode control method to suppress vibrations in a two-degree-of-freedom flexible joint manipulator, designing a control model using two subsystems to enhance the performance of traditional sliding mode control methods [12].

In summary, the above analysis indicates that current research on robot vibration suppression focuses on enhancing the dynamic performance of robots and the stability of end forces. However, for industrial welding robots, final welding quality and consistency depend on the stability of metal forming [13–15]. Research on vibration suppression in welding robots often neglects the impact of robot vibrations on the metal-forming process. Vibration suppression solely based on robot performance is insufficient to establish closed-loop control over welding quality [16]. Consequently, ensuring the stability and consistency of welding quality remains challenging.

To address the aforementioned issues, this paper proposes a novel vibration suppression method for welding robots. First, a dynamic model of the robotic welding process is established to evaluate the vibration of the welding robot. Subsequently, the joint fluctuation rate is defined to describe the vibration of each robot joint during the welding process. Based on the joint fluctuation rates, a fluctuation model of the welding pool is developed to represent and assess the impact of robot vibrations on the stability of the welding pool and the quality of welding formation. Utilizing this model, the relationship between robot vibration and welding pool stability is analyzed, and a robot welding trajectory optimization model targeting welding pool stability is created. Additionally, the Particle Swarm Optimization (PSO) algorithm is employed to optimize the welding trajectory, and a vibration suppression control strategy for welding robots is established. An experimental study on welding robot vibration suppression is then designed and conducted. The results demonstrate that the established welding pool fluctuation model can characterize the impact of robot vibration on the stability and consistency of welding quality. Furthermore, the proposed positive correlation between the vibration of each robot joint and the fluctuation of the welding pool is validated. Finally, the effectiveness of the proposed welding robot vibration suppression method is confirmed, resulting in an enhanced stability of welding formation quality.

2. Establishment of Welding Robot Model

Welding robots are developing towards the directions of intelligence, light weights, and modularization. Modular design has the advantages of a compact structure and light weight and has become the focus of welding robot development. The welding robot studied

in this paper is built by a joint module, and its shoulder joint, elbow joint and the first wrist joint are arranged in parallel, and the three wrist joints at the end are perpendicular to each other. The configuration of the welding robot is shown in Figure 1. The robot's load capacity is 5 kg, with a maximum tool end speed of 500 mm/s and a maximum joint speed of 90°/s. During welding, the end-effector speed ranges from 5 to 15 mm/s, and the end-effector acceleration ranges from 50 to 150 mm/s². Each joint has a rotational angle range of ±360°. The rated torques of the joints from the base to the end are 118 Nm, 118 Nm, 61 Nm, 13.5 Nm, 13.5 Nm, and 13.5 Nm, respectively.

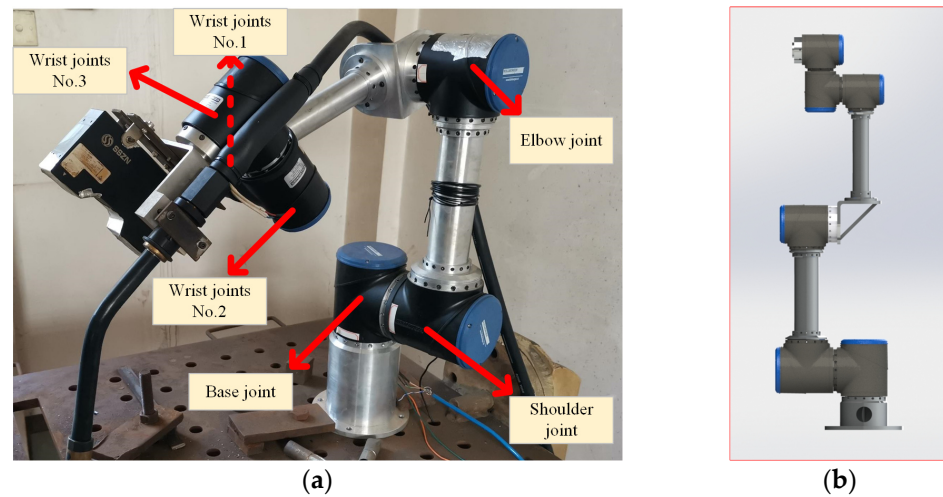


Figure 1. (a) Robot picture; (b) Robot render picture.

2.1. Vibration Equation Analysis of Welding Robot

The arc force is introduced into the dynamic model of the robot, as shown in (1).

$$M(q)\ddot{q} + C(q, \dot{q})\dot{q} + G(q) - K(\theta - q) = J^T F_{cz} \quad (1)$$

$M(q)$ is the space inertia matrix of the robot joint and $M(q) \in \mathbb{R}_{6 \times 6}$. $C(q, \dot{q})$ is the centrifugal force and Coriolis force term of the robot and $C(q, \dot{q}) \in \mathbb{R}_{6 \times 6}$. $G(q)$ is the robot gravity term and $G(q) \in \mathbb{R}_{6 \times 1}$. K is the coefficient of the permeability μ of the medium. J^T is the transfer of the Jacobi matrix for the welding robot. F_{cz} is the arc force component pointing to the weldment.

The free vibration equation of the welding robot is shown in (2).

$$M(q)\ddot{q} + C(q, \dot{q})\dot{q} + G(q) - K(\theta - q) = 0 \quad (2)$$

The variation formula is shown in (3).

$$M(q)\ddot{q} - M(q)\ddot{\theta} + C(q, \dot{q})\dot{q} + G(q) - K(\theta - q) = -M(q)\ddot{\theta} \quad (3)$$

Let q be a periodic function with a working period as the period. The coefficient of this differential equation is a function of q , so its natural frequency is also a function. Because the joint deviation of the robot is small, $|q - \theta| \leq 0.1^\circ$, and in the robot trajectory planning, the multi interpolation point interpolation algorithm will be used. However, $C(q, \dot{q})\dot{q}$ and $G(q)$ themselves are less sensitive to the changes in q and \dot{q} ; therefore, it can be considered that $C(q, \dot{q})\dot{q}$ and $G(q)$ are approximately equal between the two interpolation points, as shown in (4).

$$\begin{cases} G(q) \approx G(\theta) \\ C(q, \dot{q}) \approx C(\theta, \dot{\theta}) \end{cases} \quad (4)$$

Formula (4) can be simplified to an ordinary differential equation, as shown in (5).

$$\mathbf{M}(q)(\ddot{q} - \ddot{q}) + \mathbf{K}(q - \theta) = -\mathbf{M}(q)\ddot{\theta} - \mathbf{C}(\theta, \dot{\theta})\dot{\theta} - \mathbf{G}(\theta) \quad (5)$$

Set $q - \theta = x$. The vibration differential equation of the welding robot system is shown in (6).

$$\mathbf{M}(q)(\ddot{x}) + \mathbf{K}x = -\mathbf{M}(q)\ddot{\theta} - \mathbf{C}(\theta, \dot{\theta})\dot{\theta} - \mathbf{G}(\theta) \quad (6)$$

2.2. Extraction of Vibration Suppression Parameters

In the initial state, when solving the transient solution of the vibration equation, the displacement of the welding robot is generally not zero due to the existence of gravity, but its first and second derivatives are all zero, there is damping in the real welding robot system, and the transient response will decay quickly. Therefore, it is considered that the initial condition of the vibration equation is zero, that is, the transient solution is shown in (7).

$$y_{1r} = 0 \quad (7)$$

When solving the steady-state solution of the vibration equation, the joint motor of the welding robot will generate continuous external excitation during its movement, resulting in displacement response vibration, which is the reason for the vibration of the end effector of the welding robot. The non-homogeneous solution of the vibration equation is processed by partial integration, and the following is shown in (8).

$$x(t) = \sum_{r=0}^6 \varphi_i \frac{1}{M_{pr}\omega_r^2} \left(Q_r(t) - \int_0^t \dot{Q}_r(\tau) \cos\omega_r(t - \tau) d\tau \right) \quad (8)$$

From the formula, it can be seen that under general excitation, the vibration of the welding robot can be divided into two terms, of which the former term is a multiple of the external excitation, which is called the stable vibration term in this paper. The other item will cause the welding robot to vibrate at a high frequency, and it will change with time, so it is called the fluctuating vibration item. The stable vibration term will cause the steady-state deformation of the flexible joint due to the external excitation and the existence of the joint driving force of the welding robot. The suppression of this part of the steady-state deformation is mainly achieved by reducing the joint driving torque or reducing the welding arc force, in which the welding arc force cannot be changed, and the joint driving force can be achieved by decelerating the welding robot as a whole. The amplitude of the fluctuating vibration term varies with time, and when it reaches its maximum, it will cause great joint deformation, which will not only cause the vibration of the welding robot but also affect the motion accuracy of its end, so it needs to be suppressed. The vibration amplitude of the robot is determined by the difference between the stable vibration term and the fluctuating vibration term. Therefore, the vibration of the welding robot can be improved by changing the change rate of the external excitation, and the dimensionless quantity η is introduced as (9).

$$\eta_i = \left| \frac{\text{Fluctuating Vibration Term}}{\text{Maximum value of Stable Vibration Term}} \right| = \left| \frac{\int_0^t \dot{Q}_i(\tau) \cos\omega_i(t - \tau) d\tau}{Q_i(t)_{max}} \right| \quad (9)$$

The numerator of η is the fluctuation term, and the denominator is the maximum value of the stability term. It is defined as the vibration suppression technical parameter of the robot joint, because the number of joints of the welding robot studied in this paper is six. Therefore, the number is also six, so the displacement response of each joint of the

robot is jointly determined by six, and the more obvious the vibration of the joint is, the smaller the vibration, as shown in (10).

$$Q_i \approx -(\Phi^T M(q) \ddot{\theta})_i \quad (10)$$

The equation is taken into the general solution of the vibration equation of the flexible joint and obtained, as shown in (11).

$$x(t) = \sum_{i=0}^6 \varphi_i \frac{1}{M_{pi} \omega_i^2} \left(-(\Phi^T M(q) \ddot{\theta})_i + \int_0^t (\Phi^T M(q) \ddot{\theta})_i \cos \omega_i (t - \tau) d\tau \right) \quad (11)$$

The fluctuation term η can be obtained as shown in (12).

$$\eta_i = \left| \frac{\int_0^t (\Phi^T M(q) \ddot{\theta})_i \cos \omega_i (t - \tau) d\tau}{(J^T F_{cz} - \Phi^T M(q) \ddot{\theta})_{max}} \right| \quad (12)$$

The fluctuation term η of the welding robot is related to acceleration $\ddot{\theta}$ and acceleration $\ddot{\theta}$ inputs. Considering that the vibration of each joint of the robot affects the robot's end effector and generates a comprehensive fluctuation at the robot's end effector, this paper establishes the end effector's fluctuation based on the fluctuation rates of each joint. The vibration of each joint of the robot affects the end effector and also mutually couples when acting on the end effector. However, the degree of influence of its coupling factors can be represented by the fluctuation rates of each joint. Therefore, the end effector's fluctuation rate, denoted as η_e , can be expressed as Equation (13).

$$\eta_e = \sum_{i=1}^n \omega_i \eta_i \quad (13)$$

where ω_i is the influence weight of the vibration of each joint on the vibration of the robot's end effector, encompassing the coupling effects of other joint vibrations on the respective joint. n is the number of joints in the robot. The fluctuation η_c generated by the robotic end effector's vibration affecting the welding pool can be expressed as Equation (14).

$$\eta_c = C_1 C_2 \eta_e = C_1 C_2 \sum_{i=1}^n \omega_i \left| \frac{\int_0^t (\Phi^T M(q) \ddot{\theta})_i \cos \omega_i (t - \tau) d\tau}{(J^T F_{cz} - \Phi^T M(q) \ddot{\theta})_{imax}} \right| \quad (14)$$

where C_1 in the equation represents the comprehensive impact coefficient, indicating the extent to which the vibration at the welding torch end causes fluctuations in the welding pool. The initial value of C_1 is 1 and is associated with the welding parameters. On the other hand, C_2 stands for the fluctuation rate gain coefficient, which is related to the structure and material properties from the robot end effector to the welding torch end. It is noted that $C_2 > 1$. Generally, as the structural parameters from the robot end effector to the welding torch end increase and the stiffness and other performance parameters decrease, C_2 becomes larger, signifying a more significant impact of robot vibration on the welding pool fluctuation. In this paper, η_c is utilized to characterize the instability in the formation of the welded metal induced by robot vibration, where a larger η_c signifies a stronger instability.

3. Vibration Suppression Method Based on Trajectory Optimization

3.1. Vibration Suppression Method Based on Joint Trajectory Optimization

Taking the joint elastic potential energy of the first three joints of the welding robot as the objective function, an improved optimization algorithm based on PSO (particle swarm

optimization) is used to optimize it so as to find the joint trajectory with the smallest joint elastic potential energy and suppress the vibration of the welding machine when it locates to the welding starting point and away from the welding plane.

The PSO algorithm is an iterative optimization tool which uses particles to follow the optimal particles in the solution space for optimization search. Its concept is relatively simple, and the amount of calculation and number of parameters are less significant. After the system is initialized, it will randomly generate a group of solutions and then search the optimal solution through iterative calculation.

Vibration suppression is carried out by reducing the elastic potential energy of the joints of the welding robot, in which the control points generating the joint trajectory need to be calculated, so the dimension of the search space is equal to the number of control point increments generated by the control joint trajectory, Suppose the number of particles in the particle swarm is n . Then, the position vector of the i -th particle in the particle swarm can be expressed as $X^i = (x_{i,1}x_{i,2} \cdots x_{i,d})$, The velocity vector can be expressed as $V^i = (v_{i,1}v_{i,2} \cdots v_{i,d})$. In the process of calculation iteration, each particle of particle swarm can find the optimal solution $pbest$ according to itself, $P^i = (p_{i,1}p_{i,2} \cdots p_{i,d})$, and the optimal solution found by the whole group $gbest$, $P^g = (p_{g,1}p_{g,2} \cdots p_{g,d})$, is used to update your position and speed. Update the formula as shown in (15).

$$\begin{cases} x_{i,j}(k+1) = x_{i,j}(k) + v_{i,j}(k+1) \\ v_{i,j}(k+1) = \omega v_{i,j}(k) + c_1 rand() [p_{i,j} - x_{i,j}(k)] + c_2 rand() [p_{g,j} - x_{i,j}(k)] \end{cases} \quad (15)$$

ω is the inertia weight factor, whose value affects the global optimization ability of the algorithm, c_1 is the factor representing the self-learning ability of particles, c_2 is the factor representing the learning ability of particles to the optimal individual in particle swarm, and $rand()$ is the random number between intervals (0,1).

The working principle flow chart of the PSO algorithm is shown in Figure 2.

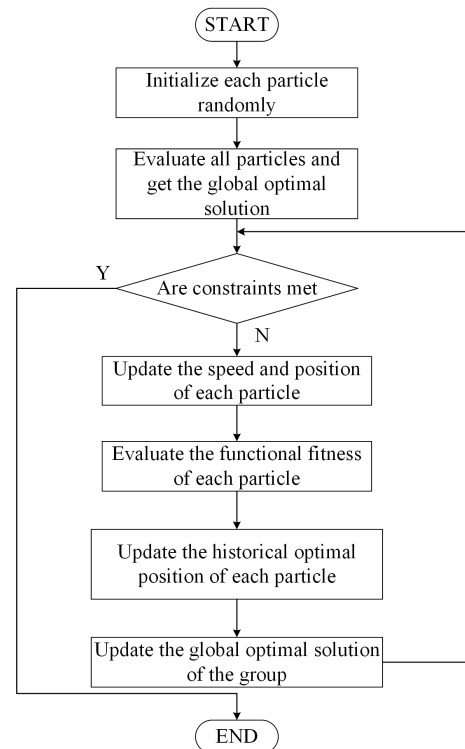


Figure 2. Control flow chart of vibration suppression method based on joint trajectory optimization; Y represents yes, and N represents no.

3.2. PSO Trajectory Optimization of the Compression Factor Based on the Penalty Function

Although the PSO algorithm with a compression factor can control the convergence of the solution and obtain a high-quality global optimal solution, it belongs to an unconstrained optimization algorithm. The particle in the particle swarm is equivalent to the increment value $\Delta\theta_i^k$ on the joint trajectory control point, and the compression factor PSO algorithm does not limit the increment value of the trajectory control point. Therefore, the calculated $\Delta\theta_i^k$ may not meet the working conditions of the robot, making the joint trajectory change greatly, which may cause accidents such as the collision of the welding robot. Therefore, the incremental value $\Delta\theta_i^k$ needs to be constrained before the PSO algorithm can be used for optimization. A constraint function is introduced to combine the objective function with the constraint conditions of the welding robot to generate a penalty function with the constraint function. The penalty function replaces the original objective function to become a new objective function, and its expression is shown in (16).

$$F(x) = f(x) + M \sum_{i=1}^m [\min(0, g_i(x))]^2 \quad (16)$$

$f(x)$ is the original objective function; in this paper, the elastic potential energy of each joint is taken, $F(x)$ is the penalty function with constraints, that is, the new objective function, M is the penalty factor of the penalty function, $g_i(x)$ is the constraints of the motion of the welding robot, and $g_i(x) \geq 0$.

The following constraints are imposed on the generation of the joint trajectory of the welding robot:

(a) Speed constraint

Each joint of the welding robot is driven by one independent motor. Because of the speed limit of the motor, the joint speed of the welding robot is also limited. If the maximum speed of the joint is $\dot{\theta}_{max}$, the joint speed of the welding robot meets the following requirements, as shown in (17).

$$F - \dot{\theta}_{max} \leq \dot{\theta}(t) \leq \dot{\theta}_{max} \quad (17)$$

(b) Torque limit

Joint modules have rated torque T_e and peak torque T_{max} , so when planning the trajectory of the welding robot, it should be considered that the torque of each joint of the robot does not exceed its peak torque. Combined with the dynamic equation, the limiting condition of robot joint torque τ can be obtained as shown in (18).

$$-\tau_{max} \leq \mathbf{M}(q)\ddot{q} + \mathbf{C}(q, \dot{q})\dot{q} + \mathbf{G}(q) \leq \tau_{max} \quad (18)$$

(c) Jerk limit

The change in jerk will cause the vibration of the joints of the welding robot, thus reducing its welding quality. Therefore, it is also necessary to take into account the constraints of trajectory optimization. Set the maximum jerk to be η_{max} .

$$0 < \eta_i = \left| \frac{\int_0^t \left(\Phi^T \mathbf{M}(q) \dot{\theta} \right)_i \cos \omega_i (t - \tau) d\tau}{\left(\mathbf{J}^T F_{cz} - \Phi^T \mathbf{M}(q) \dot{\theta} \right)_{imax}} \right| < \eta_{max} \quad (19)$$

3.3. Vibration Suppression Control Strategy of Welding Robots

Following the analysis in Section 2, it has been determined that η_c is positively correlated with η_i . When optimization leads to a decrease in η_i , it also results in a reduction in welding pool fluctuation. When it is detected that the welding robot will vibrate, it is necessary to employ corresponding vibration suppression strategies to reduce the vibration of the welding robot and improve its working accuracy. However, when the welding robot performs multi-layer and multi pass welding, its welding path is determined, so it needs to plan its trajectory in the Cartesian coordinate system. During the operation of the welding robot, a high speed is more likely to vibrate than a low speed. Therefore, a trajectory correction strategy of first decelerating, then achieving uniform speed, and then accelerating is proposed. First, the error torque of each joint of the welding robot is reduced through a deceleration process with stable acceleration changes so as to eliminate the tendency of the welding robot to vibrate. Then, a low-speed operation stage is connected with the final acceleration stage to maintain the stability of the transition between the deceleration stage and the acceleration stage of the welding robot and, at the same time, to restore the normal operation speed of the robot. In the acceleration phase of the welding robot, the torque error of each joint may also exceed the torque error threshold, forming a vibration trend and resulting in the vibration of the welding robot. Therefore, this correction strategy should also be used in the acceleration phase of the welding robot.

When the welding robot detects the vibration trend, it will decelerate according to the deceleration ratio to enter the low-speed holding stage. The motion control card will re-interpolate it according to the existing trajectory data to obtain new trajectory data and perform trapezoidal acceleration trajectory planning for the stage between the deceleration starting point and the starting point of the constant speed holding stage so as to reduce the running speed of the medium- and thick-plate welding robot, thereby achieving the effect of suppressing vibration. The welding robot is kept stable after running at a low speed for a period of time. Finally, through trapezoidal acceleration trajectory planning, the acceleration stage is carried out so that the welding robot can be accelerated to keep the total welding time unchanged, and then the welding robot can be completed, as shown in Figure 3.

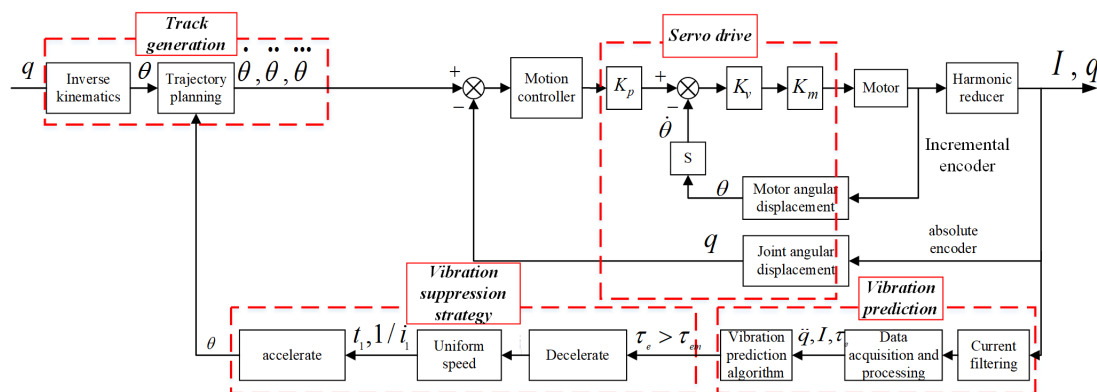


Figure 3. Track correction vibration suppression block diagram.

4. Welding Experiment

4.1. Establishment of Experimental Platform

In order to verify the vibration prediction algorithm and vibration suppression strategy proposed in the previous paper, the welding robot vibration suppression experimental platform, as shown in the figure, is built in this paper. The experimental platform is composed of a robot control system and a vibration signal acquisition system. The welding

robot control system is composed of a six-degrees-of-freedom welding robot, an upper computer, a 48 V power supply, a 24 V power supply, a motion control card, a robot control cabinet, and a welding machine. The motion control card communicates with the upper computer through the TCP/IP protocol, and the welding robot communicates with the motion control card through the EtherCAT protocol. The data exchanger of the welding machine communicates with the upper computer through the RS485 serial port and establishes communication with the welding machine through the Modbus protocol. The vibration signal acquisition system is composed of an acceleration sensor and a Ni data acquisition device. The acceleration signal is collected and processed by the Ni data acquisition device so as to analyze the vibration of the welding robot. As shown in Figure 4. In the experiment, the impact of fluctuations in current and voltage on welding quality is reduced and their consistency is maintained during the experiment.

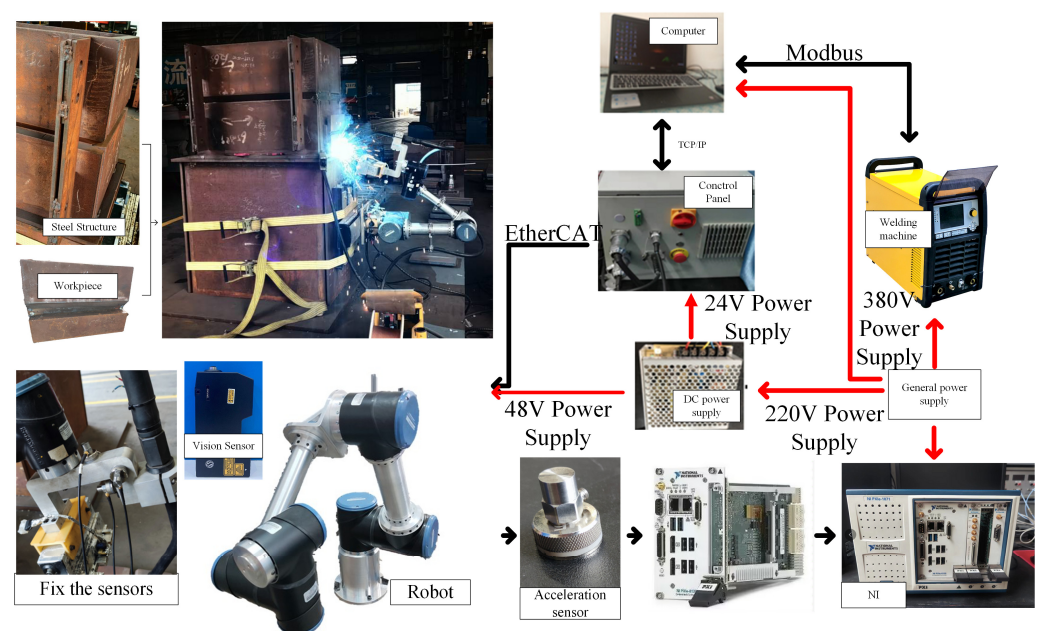


Figure 4. Welding robot experimental platform.

The vibration in the experiment is caused by the robot's movement. During the welding process, the robot moves from an extended position to a retracted position and back to an extended position. While the robot's end-effector moves at a constant speed, the joints are continuously accelerating and decelerating, making the robot unstable. Based on Equation (12), this vibration is most intense at the robot's end-effector. Since the welding torch is fixed to the end-effector, it also exhibits vibration.

As for the welding parameters, the welding mode is GMAW. The welding wire model is ER50-6 with a diameter of 1.2 mm. The welding current is set to 260 A and the voltage to 28 V. The shielding gas used is carbon dioxide, and the workpiece material is Q345 steel.

4.2. Vibration Suppression Test of Welding Robot

The automatic detection program is executed after the welding robot is set. The groove information is collected and processed by the visual sensor, and the groove characteristic parameters are extracted. The algorithm generates the welding path, and then the equipment automatically performs the welding operation. After the bottom layer welding, intermediate layer filling welding, and surface covering welding are completed in sequence, the equipment stops operation. The robot returns to a standby posture. During welding, the current information of the joint motor is detected in real time and algorithm-based-corrected and optimized to predict and suppress vibration.

4.3. Analysis of Experimental Results

In order to verify the proposed trajectory optimization vibration suppression algorithm, the compression factor PSO algorithm based on the penalty function is used to optimize the quantic polynomial joint trajectory of the end of the multi-layer and multi-pass welding robot for medium and thick plates moving from the working zero point [460, 100, 150, 180, 0, 0] to the welding starting point [550, 270, -90, 180, -5, 0]. Through the inverse kinematics calculation of the robot, the starting angle of its six joints is $[-0.4^\circ, -126.5^\circ, -120.8^\circ, -22.7^\circ, 90^\circ, -90.3^\circ]$, and the six joint angles of the multi-layer and multi-pass welding robot for medium and thick plates are $[16.7^\circ, -171.1^\circ, -77.7^\circ, -16.3^\circ, 88.6^\circ, -73.4^\circ]$ at the end. Therefore, the motion angles of the six joints of welding robot are $[17.1^\circ, -44.6^\circ, 43.1^\circ, 6.4^\circ, -1.4^\circ, 16.9^\circ]$, respectively.

Take three points with equal time intervals as control points for trajectory optimization and set the learning factor $c_1 = c_2 = 2.1$. and the compressibility factor $\partial = 0.642$. Set the number of algorithm cycles to 100, the total number of particle swarms to 100, and the penalty factor $M = 100$. Constrains the maximum value of the control increment value $\Delta\theta_i^k$ to be 2. The maximum speed is $8^\circ/\text{s}$. The optimized trajectory is shown in Figure 5.

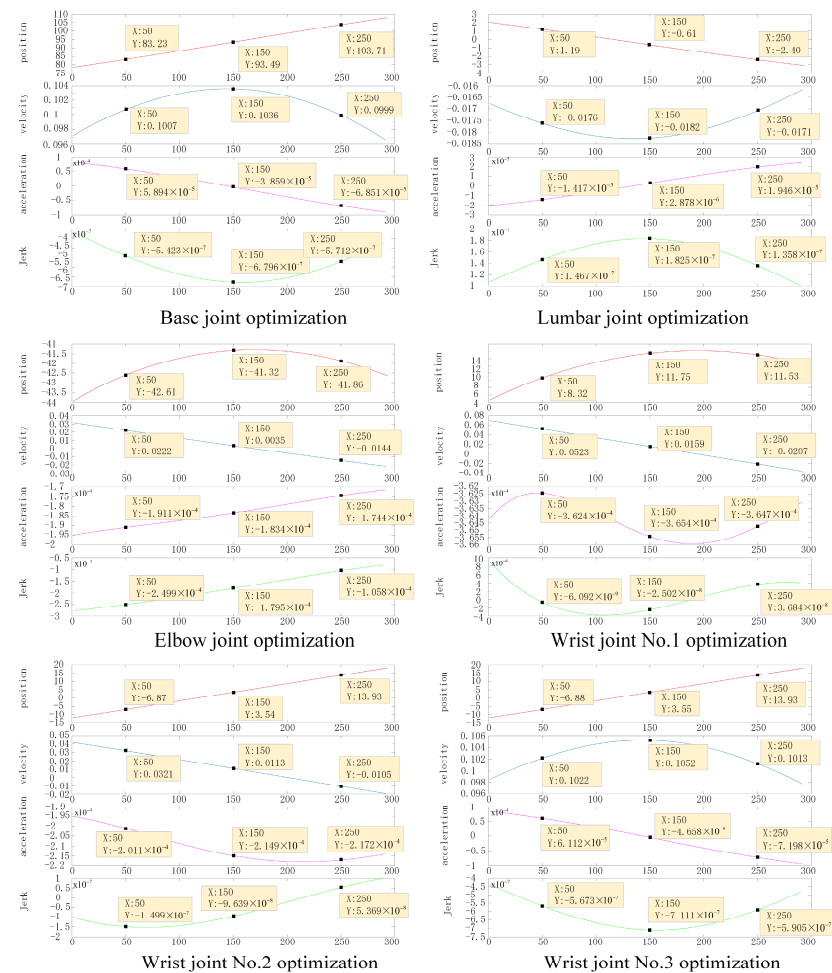


Figure 5. Optimized joint trajectory.

The current information of each joint is acquired for the same path, as shown in Figure 6. Comparing the current values of each joint motor before and after optimization in the data, we can see that the current value changes more smoothly after optimization, and the vibration of the robot is effectively suppressed.

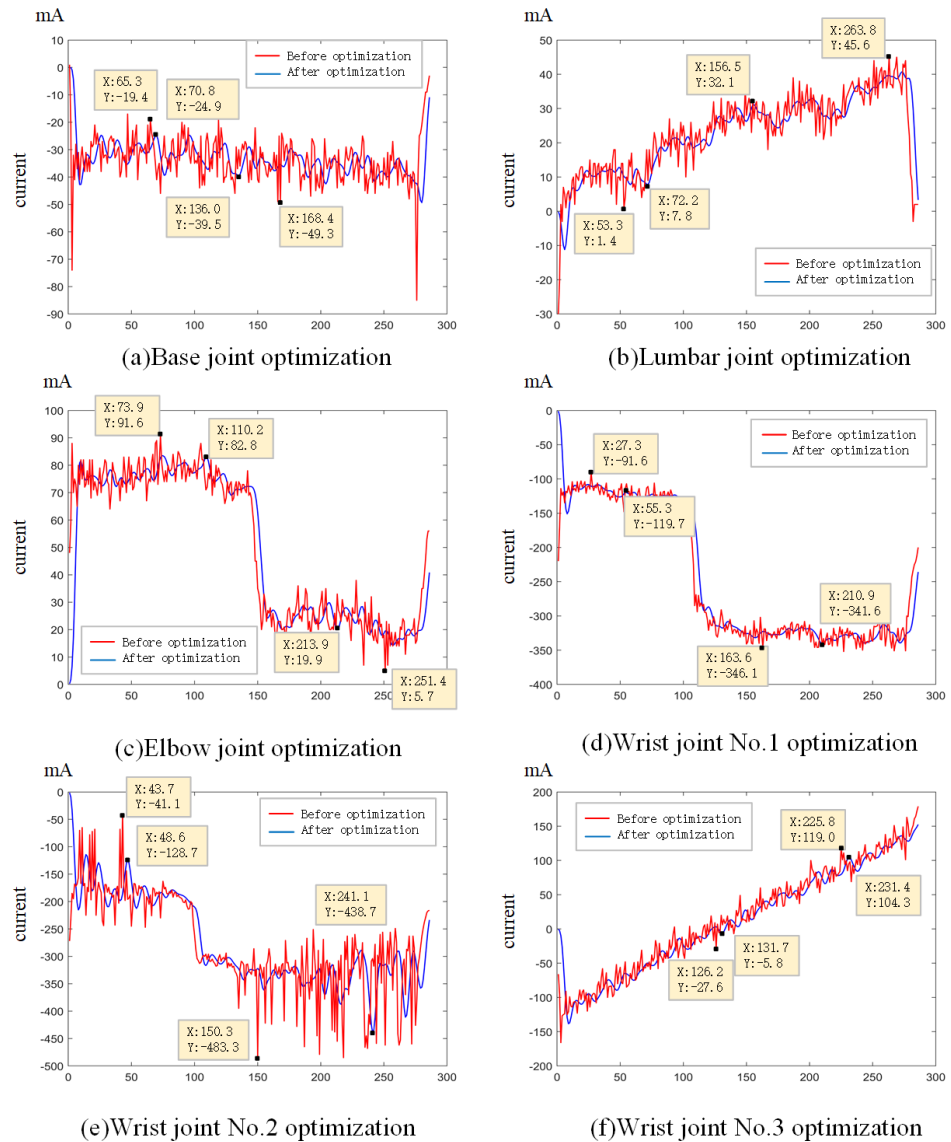


Figure 6. The current information of each joint is acquired for the same path.

Welding was performed using the trajectories both before and after optimization, and the feedback values of current and voltage were collected during the welding process. The RS485 communication protocol was used to collect data on welding current and voltage, with a sampling frequency of 50 Hz. The current and voltage before and after trajectory optimization are shown in Figure 7. The results indicate that there were significant fluctuations in the current before optimization, with sudden and severe changes, whereas no such abrupt changes were observed after optimization. Although the voltage was generally stable before optimization, there was one sudden change, which was not present after optimization. The current can be compared with the vibrations of the robot's joints shown in Figure 6. The vibrations at the robot's end-effector are mainly influenced by the three wrist joints. Among these, the second wrist joint in Figure 6 exhibits the most severe fluctuations, particularly at the start and after time 200. This corresponds to the sudden changes in current at the start and after 20 s in the welding process before optimization. Similarly, the vibration and current curves of the robot during the welding process became more stable at these points after optimization. Upon calculation, the variance and standard deviation of the current and voltage before and after trajectory optimization are shown in Table 1. The comparison shows that the variance and standard deviation of the welding

current and voltage decreased after using the trajectory optimization method proposed in this paper, indicating that the current and voltage became more stable, thereby enhancing the stability of the welding process. Compared to the vibration data of the robot joints, the experimental results for current and voltage appear less pronounced, which is due to the instability of the welding process being caused not only by robot vibrations but also by fluctuations in the current and voltage themselves.

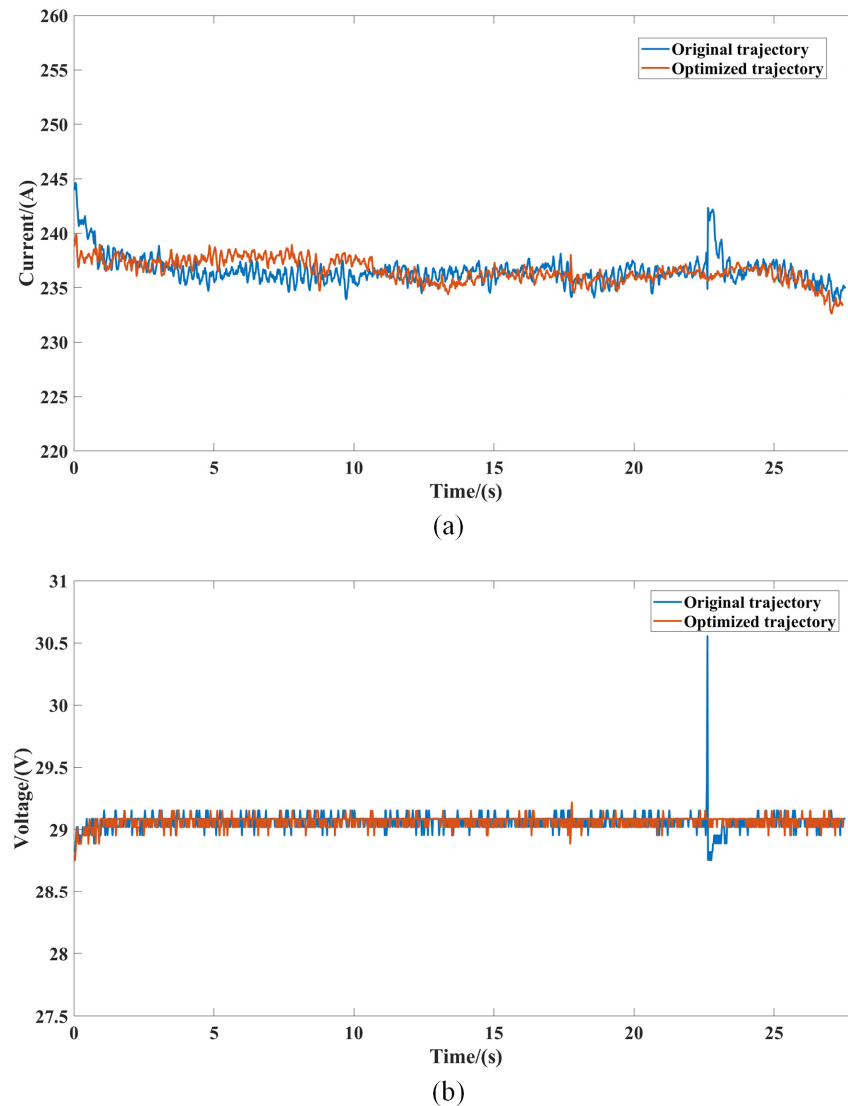


Figure 7. Welding current and voltage using the original trajectory and optimized trajectory; (a) current data; (b) voltage data.

Table 1. Variance and standard deviation of welding current and voltage before and after trajectory optimization.

Data	Variance	Standard Deviation
Current (Original trajectory)	1.5962	1.2634
Current (Optimized trajectory)	1.1547	1.0746
Voltage (Original trajectory)	0.0047	0.0685
Voltage (Optimized trajectory)	0.0020	0.0450

The welding experiment results are shown in Figure 8, where bead a and b are welds without vibration suppression implemented, and beads c, d, and e are welds for implementing vibration suppression. All five welding passes follow the same welding path and use the same welding process parameters to conduct welding experiments on a test plate.



Figure 8. Welding experiment results. The application of the proposed vibration suppression method results in the enhanced stability of welding formation quality.

5. Conclusions

This article focuses on the vibration problem during the welding process of multi-layer and multi-pass welding robots for medium and thick plates and conducts research on their vibration suppression technology. A dual threshold vibration prediction algorithm based on current feedback has been proposed, which effectively reduces the vibration during the welding process of multi-layer and multi-pass welding robots for medium and thick plates. The major findings are summarized as follows:

- (a) The dynamic equation of the multi-layer and multi-pass welding robots for medium and thick plates was established and solved. The fluctuation rate was introduced as a technical parameter for joint vibration suppression, providing constraint conditions for subsequent trajectory optimization. Based on the joint fluctuation rates, a fluctuation model of the welding pool caused by robot vibrations during the robot's welding process was established. A vibration signal processing process was designed for a multi-layer and multi-channel welding robot for medium and thick plates, facilitating the subsequent analysis of experimental data;
- (b) The compression factor PSO algorithm based on the penalty function is established to optimize the joint space trajectory of the multi-pass welding robot in order to reduce its vibration when positioned at the welding starting point and away from the welding plane. The relationship between the current and torque of the joint motor of a multi-layer and multi-channel welding robot for medium and thick plates is analyzed, and a vibration suppression response method based on trajectory correction is designed.

- (c) Welding experiments are carried out to verify the feasibility of the vibration suppression method. By processing the real-time-collected motor parameters and external sensor data during the welding process, the feasibility of suppressing the vibration of the welding robot through trajectory optimization and vibration prediction and response was verified.

Factors affecting the stability of the welding process include robot vibrations and fluctuations in current and voltage, with the impact of robot vibrations remaining significant. The method proposed in this paper proactively reduces vibrations through an algorithmic approach. For each welding trajectory, the model proposed in this paper can assess its vibration level. Therefore, in industrial production, this vibration model can be used to evaluate vibrations, achieving the purpose of predicting vibrations. When the vibration level exceeds the limit, the vibration suppression algorithm proposed in this paper can be used to optimize the welding trajectory to reduce vibrations.

Author Contributions: Conceptualization, H.L., M.M. and Y.Z.; methodology, M.M. and Z.W.; software, Z.W. and H.H.; validation, X.Y., X.F. and M.M.; formal analysis, M.M., Z.L. (Zhi Liu) and Z.L. (Zhangjie Li); writing—original draft preparation, M.M. and Z.W.; writing—review and editing, Y.Z. and H.L. All authors have read and agreed to the published version of the manuscript.

Funding: This research was supported by the Key Research and Development project of Hubei Science and Technology Plan [Project No.: 2024BAB055], the Key Research and Development project of Hubei Science and Technology Plan [Project No.: 2023BEB013], and the Hubei Provincial Science and Technology Innovation Talent Project [No. 2023DJC060].

Institutional Review Board Statement: Not applicable.

Informed Consent Statement: Not applicable.

Data Availability Statement: Data can be found in the manuscript.

Conflicts of Interest: Author Yongquan Zhang was employed by the company Hubei Tuansteel Science and Technology Research Co., Ltd. (Part time). The remaining authors declare that the research was conducted in the absence of any commercial or financial relationships that could be construed as a potential conflict of interest.

References

1. Curiel, D.; Veiga, F.; Suarez, A.; Villanueva, P. Advances in Robotic Welding for Metallic Materials: Application of Inspection, Modeling, Monitoring and Automation Techniques. *Metals* **2023**, *13*, 711. [[CrossRef](#)]
2. Ribeiro, J.; Lima, R.; Eckhardt, T.; Paiva, S. Robotic Process Automation and Artificial Intelligence in Industry 4.0—A Literature review. *Procedia Comput. Sci.* **2021**, *181*, 51–58. [[CrossRef](#)]
3. Feng, X.; Tian, W.; Wei, R.; Pan, B.; Chen, Y.; Chen, S. Application of a Wall-Climbing, Welding Robot in Ship Automatic Welding. *J. Coast. Res.* **2020**, *106*, 609. [[CrossRef](#)]
4. Li, Y.; Tong, B.A.; Chen, W.B.; Li, X.Y. Performance Margin Modeling and Reliability Analysis for Harmonic Reducer Considering Multi-Source Uncertainties and Wear. *IEEE Access* **2020**, *8*, 171021–171033. [[CrossRef](#)]
5. Liu, X.; Jiang, D.; Tao, B.; Jiang, G.; Sun, Y.; Kong, J.; Tong, X.; Zhao, G.; Chen, B. Genetic algorithm-based trajectory optimization for digital twin robots. *Front. Bioeng. Biotechnol.* **2020**, *9*, 793782. [[CrossRef](#)]
6. Villani, V.; Pini, F.; Leali, F.; Secchi, C. survey on human-robot collaboration in industrial settings: Safety, intuitive interfaces and applications. *Mechatronics* **2018**, *55*, 248–266. [[CrossRef](#)]
7. Shi, Y.; Li, C.; Huang, Y. Resonance suppression of a controllable mechanism welding robot end with central composite design methodology. *Appl. Sci.* **2022**, *12*, 6352. [[CrossRef](#)]
8. Balaji, P.S.; Karthik SelvaKumar, K. Applications of nonlinearity in passive vibration control: A review. *J. Vib. Eng. Technol.* **2021**, *9*, 183–213. [[CrossRef](#)]
9. Yuan, X.; Lu, H.; Zhang, Y.; Chen, Z.; Wu, Z.; Zhou, T.; Huang, H.; Fu, H. A Vibration Suppression Control Strategy Based on Grey Wolf Optimization Algorithm. In Proceedings of the ICMD: International Conference on Mechanical Design, Chengdu, China, 20–22 October 2023; Springer Nature: Singapore, 2023; pp. 1143–1159.
10. Li, D.; Du, L. Auv trajectory tracking models and control strategies: A review. *J. Mar. Sci. Eng.* **2021**, *9*, 1020. [[CrossRef](#)]

11. Fabritius, M.; Kraus, W.; Pott, A. Improving the Accuracy of Cable-Driven Parallel Robots Through Model Optimization and Machine-Learning. In Proceedings of the IFToMM World Congress on Mechanism and Machine Science, Tokyo, Japan, 5–10 November 2023; Springer Nature: Cham, Switzerland, 2023; pp. 565–576.
12. Rsetam, K.; Cao, Z.W.; Man, Z.H. Design of Robust Terminal Sliding Mode Control for Underactuated Flexible Joint Robot. *IEEE Trans. Syst. Man Cybern.-Syst.* **2023**, *52*, 565–576. [[CrossRef](#)]
13. Hirano, D.; Fujii, Y.; Abiko, S.; Lampariello, R.; Nagaoka, K.; Yoshida, K. Vibration suppression control of a space robot with flexible appendage based on simple dynamic model. In Proceedings of the 2013 IEEE/RSJ International Conference on Intelligent Robots and Systems, Tokyo, Japan, 3–7 November 2013; pp. 6631–6637.
14. Zhu, W.-Q. Typical dielectric elastomer structures: Dynamics and application in structural vibration control. *J. Zhejiang Univ. Sci. A Appl. Phys. Eng.* **2016**, *17*, 335–352.
15. Trung, T.V.; Iwasaki, M. H_∞ Control-based Vibration Suppression in Robot Arm with Strain Wave Gearing. In Proceedings of the 2018 International Power Electronics Conference (IPEC-Niigata 2018-ECCE Asia), Niigata, Japan, 20–24 May 2018; pp. 1666–1672.
16. Cui, L.; Wang, H.; Chen, W. Trajectory planning of a spatial flexible manipulator for vibration suppression. *Robot. Auton. Syst.* **2020**, *9*, 183–213. [[CrossRef](#)]

Disclaimer/Publisher’s Note: The statements, opinions and data contained in all publications are solely those of the individual author(s) and contributor(s) and not of MDPI and/or the editor(s). MDPI and/or the editor(s) disclaim responsibility for any injury to people or property resulting from any ideas, methods, instructions or products referred to in the content.